Available online at www.sciencedirect.com

SCIENCE DIRECT®

Remote Sensing of Environment 98 (2005) 63 – 79

Remote Sensing of Environment

www.elsevier.com/locate/rse

A simple and effective radiometric correction method to improve landscape change detection across sensors and across time

Xuexia Chen [a,*], Lee Vierling [a,1], Don Deering [b]

[a] *Institute of Atmospheric Sciences, South Dakota School of Mines and Technology, Rapid City, South Dakota 57701, United States*
[b] *NASA Goddard Space Flight Center, Greenbelt, Maryland 20771, United States*

Received 15 August 2004; received in revised form 21 April 2005; accepted 18 May 2005

Abstract

Satellite data offer unrivaled utility in monitoring and quantifying large scale land cover change over time. Radiometric consistency among collocated multi-temporal imagery is difficult to maintain, however, due to variations in sensor characteristics, atmospheric conditions, solar angle, and sensor view angle that can obscure surface change detection. To detect accurate landscape change using multi-temporal images, we developed a variation of the pseudoinvariant feature (PIF) normalization scheme: the temporally invariant cluster (TIC) method. Image data were acquired on June 9, 1990 (Landsat 4), June 20, 2000 (Landsat 7), and August 26, 2001 (Landsat 7) to analyze boreal forests near the Siberian city of Krasnoyarsk using the normalized difference vegetation index (NDVI), enhanced vegetation index (EVI), and reduced simple ratio (RSR). The temporally invariant cluster (TIC) centers were identified via a point density map of collocated pixel VIs from the base image and the target image, and a normalization regression line was created to intersect all TIC centers. Target image VI values were then recalculated using the regression function so that these two images could be compared using the resulting common radiometric scale. We found that EVI was very indicative of vegetation structure because of its sensitivity to shadowing effects and could thus be used to separate conifer forests from deciduous forests and grass/crop lands. Conversely, because NDVI reduced the radiometric influence of shadow, it did not allow for distinctions among these vegetation types. After normalization, correlations of NDVI and EVI with forest leaf area index (LAI) field measurements combined for 2000 and 2001 were significantly improved; the r^2 values in these regressions rose from 0.49 to 0.69 and from 0.46 to 0.61, respectively. An EVI "cancellation effect" where EVI was positively related to understory greenness but negatively related to forest canopy coverage was evident across a post fire chronosequence with normalized data. These findings indicate that the TIC method provides a simple, effective and repeatable method to create radiometrically comparable data sets for remote detection of landscape change. Compared to some previous relative radiometric normalization methods, this new method does not require high level programming and statistical skills, yet remains sensitive to landscape changes occurring over seasonal and inter-annual time scales. In addition, the TIC method maintains sensitivity to subtle changes in vegetation phenology and enables normalization even when invariant features are rare. While this normalization method allowed detection of a range of land use, land cover, and phenological/biophysical changes in the Siberian boreal forest region studied here, it is necessary to further examine images representing a wide variety of ecoregions to thoroughly evaluate the TIC method against other normalization schemes.

Keywords: Relative radiometric normalization; Post-fire chronosequence; Boreal forest; Temporally invariant cluster; Leaf area index; Enhanced vegetation index; Normalized difference vegetation index; Reduced simple ratio; Landscape detection

* Corresponding author. Current address: Science Applications International Corporation (SAIC), Contractor to the USGS National Center for Earth Resources Observation and Science (EROS), 47914 252nd Street, Sioux Falls, South Dakota 57198, United States.
E-mail addresses: xuchen@usgs.gov (X. Chen), leev@uidaho.edu (L. Vierling), Donald.W.Deering@nasa.gov (D. Deering).
[1] Current address: College of Natural Resources, University of Idaho, Moscow, Idaho, 83844, United States.

0034-4257/$ - see front matter © 2005 Elsevier Inc. All rights reserved.
doi:10.1016/j.rse.2005.05.021

1. Introduction

1.1. Landscape change detection with multi-temporal imagery

Detection and quantification of surface change lie at the heart of satellite remote sensing. Proper timing and intercomparison of satellite image acquisitions, therefore, are often central to terrestrial studies ranging in scope from understanding natural and anthropogenic disturbance regimes to quantifying climate-driven shifts in vegetation biogeography and phenology. Changes of interest range in magnitude from major, easily detectable transformations large in grain size (such as urbanization and forest clearing, e.g. Skole & Tucker, 1993) to more subtle differences arising from slight changes in green leaf area (e.g. Chen & Cihlar, 1996; Myneni et al., 1997; Spanner et al., 1994). Regardless of the magnitude of the change process of interest, careful considerations must be made when comparing multi-temporal remote sensing imagery (Roughgarden et al., 1991). Radiometric consistency among ground targets in multi-temporal imagery is difficult to maintain due to changes in sensor characteristics, atmospheric condition, solar angle, and sensor view angle (Du et al., 2002; Lillesand & Kiefer, 1994). Therefore, radiometric corrections are often performed on multi-temporal imagery to reduce any or all of the above influences and increase sensitivity to landscape change (e.g. Chavez, 1996; Chen et al., 2004; Coppin et al., 2004; Roderick et al., 1999; Song et al., 2001; Spanner et al., 1994). In this paper, we describe the development of a new relative radiometric normalization technique for landscape-level change detection, and apply this technique to study anthropogenic and post-fire landscape change in southern Siberia.

1.2. Radiometric correction methods

Two types of radiometric corrections, absolute correction and relative correction, are commonly employed to normalize remotely sensed images for time-series intercomparison (e.g. Cohen et al., 2003b; Coppin et al., 2004; Du et al., 2002; Elvidge et al., 1995; Kaufman, 1988; Schott, 1997; Schott et al., 1988; Song et al., 2001). Absolute radiometric correction is aimed towards extracting the absolute reflectance of scene targets at the surface of the earth. This method requires the input of simultaneous atmospheric properties and sensor calibration, which are difficult to acquire in many cases, especially in historic data (Chavez, 1996; Du et al., 2002; Song et al., 2001; Spanner et al., 1990). Relative radiometric correction is aimed towards reducing atmospheric and other unexpected variation among multiple images by adjusting the radiometric properties of target images to match a base image (Hall et al., 1991), thus it is also called relative radiometric normalization. Relative radiometric normalization is an image based correction method achieved by setting the multi-temporal images into a common scale without extra parameters from other measurements. In this method, reflectance of invariant targets within multiple scenes can be used to render the scenes to appear as if they were acquired with the same sensor, with the same calibration, and under identical atmospheric conditions, without the need to be absolutely corrected to surface reflectance.

Most relative methods assume that radiometric relationships between the target image and the base image are linear (Du et al., 2002; Elvidge et al., 1995; Schott et al., 1988; Song et al., 2001). A base image, selected to represent some common scale, is not required to be the most accurate reflectance estimation (Song et al., 2001). The relative radiometric normalization method can correct noise deriving from the atmosphere, sensor, and other sources in one process, and is therefore widely used. Generally, relative normalization methods are simpler than absolute normalization methods, and some relative methods can detect land cover changes as well as when high accuracy absolute radiometric corrections are employed (e.g. Andrefouet et al., 2001; Song et al., 2001).

It should be noted that radiometric normalization is not always necessary for multi-temporal satellite image intercomparison. For example, it is not necessary to perform normalizations if the land cover classification method for multiple images is based on the spectral signals from each individual image (Song et al., 2001). Below, we summarize radiometric correction methods used in some previous studies.

1.2.1. Absolute radiometric correction

Generally, absolute radiometric correction is a two-step process. The first step is to convert the digital number (DN) of the sensor measurements to spectral radiance measured by satellite sensors using Eq. (1).

$$L_{\text{sat}} = DN \times Gain + Offset \tag{1}$$

Here L_{sat} is spectral radiance detected by a satellite sensor; DN is the digital number of the sensor measurement, and Gain and Offset are sensor-specific calibration parameters determined prior to sensor launch. While these parameters are usually assumed to be stable, they can change due to long-time service or accidents (Schowengerdt, 1997).

The second step of absolute radiometric correction is to transfer the sensor detected radiance into ground surface reflectance using Eq. (2) (Lillesand & Kiefer, 1994).

$$\rho_{\text{surface}} = \frac{\left(L_{\text{sat}} - L_{\text{path}}\right)\pi}{E\tau} \tag{2}$$

Here ρ_{surface} is the ground surface reflectance of the target. L_{path} is the path radiance, E is the irradiance on the ground target, and τ is the transmission of the atmosphere (Lillesand & Kiefer, 1994). Absolute radiometric models use in situ measurements or reasonable estimation of

atmospheric optical depth, solar zenith angle and satellite status to input parameters for calculating the ground surface reflectance (e.g. Chavez, 1996; Song et al., 2001).

1.2.2. Relative radiometric correction

1.2.2.1. Dark Object Subtraction (DOS) method. In an ideal situation, a radiometrically "dark" object produces zero radiance in all wavelengths. In the Dark Object Subtraction (DOS) method, it is assumed that any radiance received at the sensor for a dark object pixel is due to atmospheric path radiance (Chavez, 1996). Thus, for dark objects, the pixels containing the lowest DN values are selected from the image and their representative value is subtracted from the DNs across the whole scene to reduce scattering influences. The dark objects need to be carefully chosen from the scene; clear water bodies and dark vegetation under shadows are traditionally selected as dark objects (e.g. Chavez, 1996; Song et al., 2001). DOS is a simple method and has been widely used in many applications, though the accuracy of DOS might not be acceptable in some applications because while this method can correct atmospheric scattering effects, it can not correct for differential atmospheric transmittance (Chavez, 1996). Some expanded DOS methods incorporate the cosine of the solar zenith angle or atmospheric aerosol effects to improve the accuracy of the atmospheric transmittance correction (Chavez, 1996; Song et al., 2001).

1.2.2.2. Pseudoinvariant Features (PIF) methods. Schott et al. (1988) developed a relative radiometric normalization method using spectrally pseudoinvariant features, such as impervious roads, roof tops and parking lots, to allow intercomparisons between a target image and a base image by calculating an image based linear regression. In this method, red and near infrared scatter plots are used to create a pseudoinvariant features (PIF) mask image containing only urban features for each image. Histogram statistics of the two mask images are then generated to create band-by-band transforms for the radiometric correction. Shortcomings of this method include the fact that moisture changes in PIF can influence the accuracy of the approach (Salvaggio, 1993; Schott et al., 1988) and the accuracy of isolating the pseudoinvariant features depends on the user's ability and knowledge (Schott, 1997). It has been noted that in this method the invariant features are not required to be collocated pixels (Elvidge et al., 1995).

Elvidge et al. (1995) also created a relative radiometric normalization method using an automatic scattergram controlled regression (ASCR) algorithm to identify invariant regions and compute regression lines for radiometric correction. This method uses scattergrams and histograms of near infrared bands to identify invariant pixels. Large areas of land and water features containing significant reflectance differences in near infrared bands are required to apply this method. Thus, application of this method is limited in scenes that contain only one peak in the near infrared histogram.

Du et al. (2002) also developed an improved method for PIF selection. With this method, PIFs are selected via principal component analysis (PCA) using the scatter plots of two images. A linear regression function for relative radiometric normalization is created by objective statistics calculation based on the PIFs. Finally, quality control of the normalized image is conducted to ensure the accuracy of the radiometric correction (Du et al., 2002). This method requires advanced levels of programming and statistical skills for appropriate use.

1.2.2.3. Ridge method. The ridge method was first suggested by Robert Kennedy and Warren Cohen, and first described and applied by Song et al. (2001). This method uses a density plot of all pixels collocated in two images acquired on different dates to identify the linear normalization function. The axes of the density map represent the DN values of collocated pixels in the respective images. In the density plot, the invariant pixels in two images cluster together to form a high density ridge that is used to calculate a linear regression function to normalize the target image. If the scene contains areas of pronounced variation, such as those influenced by clouds and land cover changes, the variant pixels should be excluded from the density plot (Song et al., 2001). The accuracy of this simple method is comparable to that of some complex absolute normalization methods, and as a result has seen much recent use (e.g. Andrefouet et al., 2001; Cohen et al., 2003a,b; Song et al., 2001). The shortcoming of this method is that the identification of a regression function is based on the visual observation of the density ridge. If most of the collocated pixels contain subtle and systemic changes due to factors such as phenological responses to different growth seasons, the density ridge may contain biased distortions and the regression function may be difficult to identify or will contain bias errors. Subtle landscape changes can be "normalized away" in the process if most pixels exhibit similar changes between observations. More discussion of the ridge method is presented later in this paper.

1.3. Objectives

The goal of this study is to develop an improved PIF relative radiometric normalization method for remote change detection, using multi-temporal imagery of a post-fire chronosequence in southern Siberia as a test case. Siberian boreal forest ecosystems represent complex mosaics where several agents of change (e.g. climate change, forest fires, insects, and human activities) co-occur. As this study is part of a larger effort to understand post-fire vegetation dynamics in conifer systems (Deering et al., in preparation) we: (1) describe the methodology and assumptions of a newly developed temporally invariant cluster (TIC) relative radiometric normalization

method; (2) normalize vegetation indices using this TIC method; (3) use normalized NDVI and EVI data to interpret field leaf area index (LAI) collected at sites representing a post-fire chronosequence; and (4) describe and interpret the NDVI and EVI dynamics of the boreal region encompassed by the imagery (including deciduous forests, conifer forests, unforested pasture and cropland, and sparsely vegetated human settlements) all occurring within a mosaic of various anthropogenic disturbance regimes and post-fire ages.

2. Methodology

2.1. Study sites and data collection

The study area is located northwest of the Siberian city of Krasnoyarsk (57.3°N, 91.6°E), Russia in the Krasnoyarsk Kray of central Siberia (Fig. 1). Mixed conifer forests consisting of spruce (*Picea obovata*), fir (*Abies sibirica*), and Siberian pine (*Pinus sibirica*) are the dominant land cover. Hardwood stands of birch (*Betula pendula*) and aspen (*Populus tremuloides*) are also present, typically occurring as early- to mid-successional post-disturbance vegetation community. The understory in this area is mainly comprised of a mixture of grasses, forbs, and deciduous shrubs.

Four sites for field data collection were established in the study area with multiple post-fire ages in 2000: 1 year (1999 burn), 13 years (1987 burn), 24 years (1976 burn), and over 100 years (Table 1, Fig. 2). These sites include conifer and deciduous forests and also cross a wide range of post-fire age; thus they serve as a post-fire chronosequence.

Four to six 25 by 25 m plots were established within each study site. These plots covered a wide range of overstory LAI in each study site. Field data were collected in the summers of 1999, 2000 and 2001 (Table 1) including LI-COR LAI-2000 (Lincoln, NE), TRAC (Tracing Radiation and Architecture of Canopies, 3rd Wave Engineering, Nepean, Canada), ground cover, canopy cover, plot diagrams (tree species, location, and diameter at breast height), selected hemispherical photos, and limited destructive sampling. In this study we used the field LAI derived from LAI-2000 measures in 2000 and 2001 to compare with satellite data collected in those two summers.

Table 1
Description of field sites

Post-fire age in 2000 (yr)	Fire occurred	Predominant vegetation	Latitude	Longitude	Field data collection time
1	1999	Mixed dark coniferous	57°16′N	91°37′E	1999 2000 2001
13	1987	Young deciduous broadleaf	57°34′N	91°32′E	2000
24	1976	Deciduous broadleaf	56°57′N	91°33′E	2001
100+	Before 1900	Mixed dark coniferous	57°16′N	91°37′E	1999 2000 2001

In this study, three Landsat images were selected for analyses, including one Landsat 4 image (acquired 9 June 1990) and two Landsat 7 ETM+ images (acquired 20 June 2000, and 26 August 2001). All images were of good quality with <10% cloud over. The region of interest (34 × 78 km) for image analysis is shown as a rectangle on the satellite scene in Fig. 2. Between 1990 and 2000, there was a significant land cover change from forest to crop/pasture lands, while the 2001 image contained a cloud and cloud shadow within the area of interest (Fig. 3). These changes each represented <10% of the analysis area. In addition, an IKONOS image (1 m resolution panchromatic data; 4 m resolution multispectral data) was collected on 23 June 2000 above the two conifer study sites. The IKONOS image provided detailed information of the surface and helped to interpret the surface features detected by the Landsat images. Satellite image acquisitions and field data

Fig. 1. Study area in Krasnoyarsk Kray, Russia. The general field site is denoted as a circle.

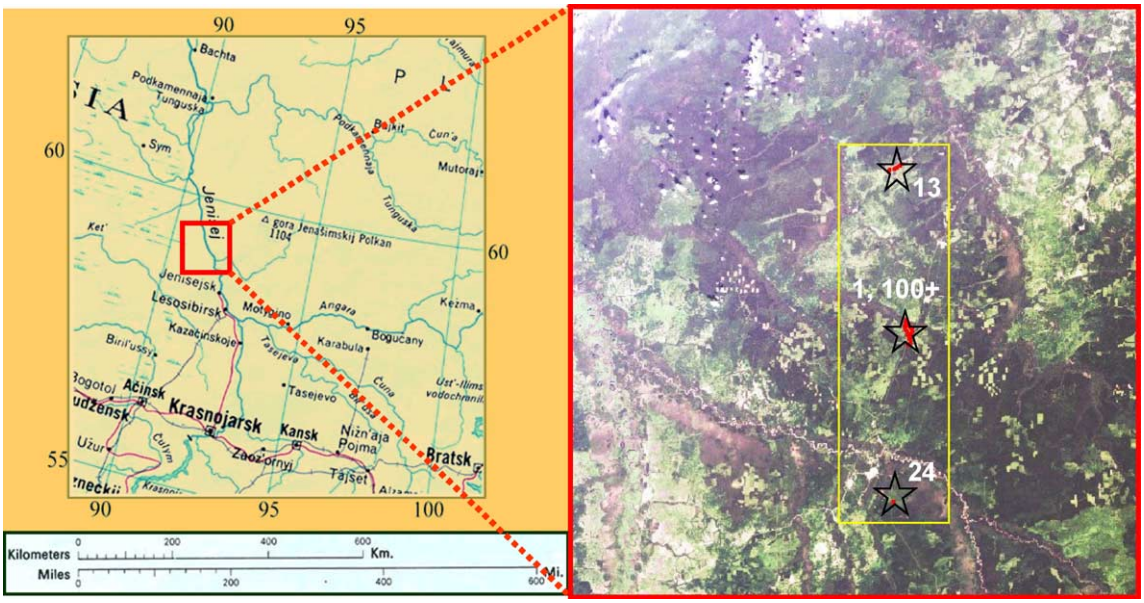

Fig. 2. Field data collection sites of multiple post-fire ages (13, 1, 100+, and 24 years) in 2000. The region of interest for image analysis measures 34 × 78 km and is marked as a rectangle on a 2000 Landsat 7 image.

collection dates were planned so as to allow for meaningful intercomparison.

2.2. Image processing

To keep an agreement of pixel size between the two Landsat sensors, the Landsat 4 1990 image was resampled to a 30 m pixel size from its original 28.5 m resolution using bilinear resampling. Comparison between field GPS records of road entrance points with road features in Landsat images indicated that the Landsat 7 2000 image contained the highest accuracy with ground measurements. Thus the 2000 image was used as the base image for geo-registration of the other two images acquired in 1990 and 2001.

Raw image data were converted to at satellite reflectance, and dark object subtractions were performed on each image to reduce the influence of atmospheric scattering within each scene. Vegetation indices, including normalized difference vegetation index (NDVI), enhanced vegetation index (EVI) and reduced simple ratio (RSR) were calculated for each image based on the equations described below.

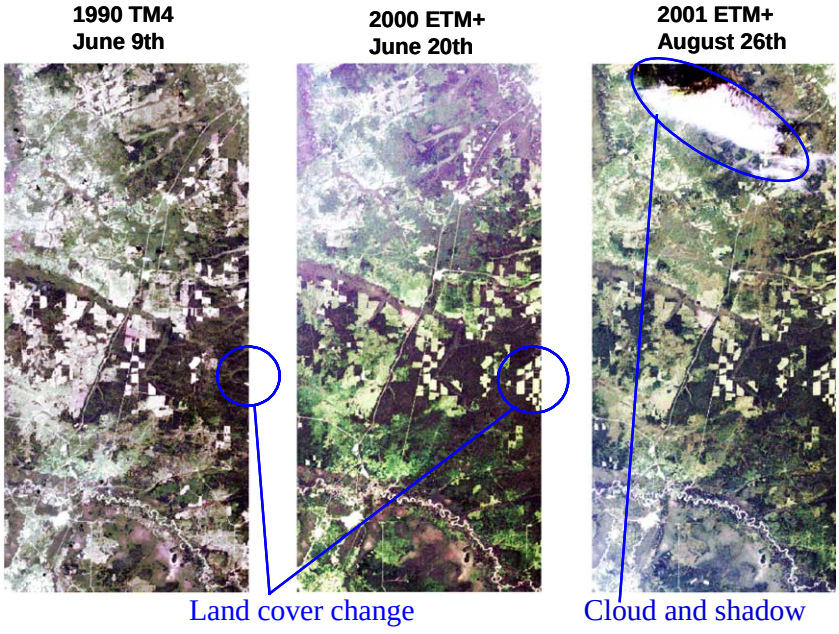

Fig. 3. Region of interest subset images in 1990, 2000, and 2001 (34 × 78 km), with key landscape changes indicated.

2.3. Spectral vegetation indices

Because we are most interested in studying vegetation-related changes in and around post-fire sites, spectral vegetation indices (SVIs) were employed in this study in order to track landscape change. The SVIs of interest include NDVI, EVI, and RSR.

The normalized difference vegetation index (NDVI) is a traditional vegetation index and is calculated by using the reflectance in the red and near infrared bands (Rouse et al., 1974) so that

$$NDVI = \frac{\rho(\lambda_{NIR}) - \rho(\lambda_{red})}{\rho(\lambda_{NIR}) + \rho(\lambda_{red})}. \quad (3)$$

Where $\rho(\lambda_{red})$ and $\rho(\lambda_{NIR})$ are the reflectance in red and near infrared respectively. NDVI can reduce atmospheric and illumination influences using the difference and ratio of red and near infrared bands (Schott, 1997). NDVI has been widely used in a tremendous body of remote sensing research.

The more recently developed enhanced vegetation index (EVI) can minimize the influences of canopy background and atmospheric variation better than can NDVI (Huete et al., 2002; Miura et al., 2001). EVI is calculated by using the reflectance of blue, red and near infrared bands (Huete et al., 2002; Miura et al., 2001) so that

$$EVI = G\frac{\rho(\lambda_{NIR}) - \rho(\lambda_{red})}{\rho(\lambda_{NIR}) + C_1\rho(\lambda_{red}) - C_2\rho(\lambda_{blue}) + L}. \quad (4)$$

Where L is a canopy background adjustment factor based on the nonlinear extinction of red and NIR wavelengths through the canopy, C_1 and C_2 are the adjustment factors for aerosol influences, and G is a gain factor for the whole equation (Huete et al., 1997). Huete et al. (1997) suggested parameters for EVI to be $L=1$, $C_1=6$, $C_2=7.5$, and $G=2.5$.

The reduced simple ratio (RSR) is a vegetation index containing an additional shortwave infrared (SWIR) term for better derivation of LAI (Chen et al., 2002). It is calculated by using the red, near infrared and shortwave infrared reflectance (Brown et al., 2000) so that

$$RSR = \frac{\rho(\lambda_{NIR})}{\rho(\lambda_{red})}\left[1 - \frac{\rho(\lambda_{SWIR}) - \rho(\lambda_{SWIR_{min}})}{\rho(\lambda_{SWIR_{max}}) - \rho(\lambda_{SWIR_{min}})}\right]. \quad (5)$$

Where $\rho(\lambda_{red})$, $\rho(\lambda_{NIR})$, and $\rho(\lambda_{SWIR})$ are the reflectances in red, near infrared, and shortwave infrared bands. $\rho(\lambda_{SWIR_{min}})$ and $\rho(\lambda_{SWIR_{max}})$ are the 1% minimum and maximum reflectance in the whole scene respectively (Chen et al., 2002).

Spanner et al. (1990) demonstrated that path radiance accounted for about 50% of the radiance in the TM red band, 20% in the near infrared and less than 10% in the SWIR. Thus it is not a surprise that EVI is less sensitive to atmospheric contamination than is the NDVI, as it is designed to contain the correction of canopy background and atmospheric scattering influences (Gao et al., 2000; Xiao et al., 2003). In calculating RSR, the SWIR (TM band 5) was used to normalize the influence of vegetation cover types and the background (e.g. understory, soil) so that RSR greatly improved LAI retrieval in mixed forest (Chen et al., 2002). In this study, we develop and use the temporally invariant cluster (TIC) method to normalize the NDVI, EVI, and RSR for multi-temporal change detection in these post-fire environments.

2.4. The Temporally Invariant Cluster (TIC) method

The goal of relative radiometric normalization is to remove or reduce the variance deriving from effects other than surface change. The temporally invariant cluster (TIC) method is based on the following two assumptions. During the multi-temporal collocated observations:

(1) There are at least two invariant surface features with spectral characteristics that can be significantly distinguished from each other and other variant pixels.
(2) The radiometric relationships of invariant pixels in the images are linear, and the atmosphere is homogeneous across the extent of each scene.

The second assumption has been generally accepted in previous studies of band-by-band normalization (e.g. Du et al., 2002; Elvidge et al., 1995; Schott et al., 1988; Song et al., 2001). In this study we normalize the vegetation indices directly instead of using band-by-band normalization. In the study by Myneni and Asrar (1994) of atmospheric effects and spectral vegetation indices, the atmospheric influence upon several vegetation indices, including NDVI, SAVI, ARVI (atmospherically resistant vegetation index), and SARVI (soil and atmospherically resistant vegetation index) were close to linear. In addition, a strong linear correlation of EVI and SAVI ($r^2=0.99$) was found in a study of Gao et al. (2000). Thus, radiometric correlations of NDVI and EVI among multi-temporal images are assumed to be linear in this study. The TIC method was used to normalize vegetation indices including NDVI and EVI derived from 1990, 2000 and 2001 Landsat 4 TM and Landsat 7 ETM+ data in Siberian boreal forests. To understand normalization issues that may be encountered as a result of nonlinearity, we also conducted pilot analyses using the RSR, which has been shown to vary nonlinearly with changes in atmospheric conditions.

The methodology of the TIC method is comprised of the following four steps:

(1) Using georegistered imagery, input data from both base and target images to a scatter plot. The x- and y-axes of the scatter plot represent the vegetation index values of collocated pixels between both scenes.
(2) Create a point density map based on the scatter plot. According to the two assumptions described above, at least two temporally invariant cluster (TIC) centers in the density map must be spectrally distinct.

(3) Identify the normalization regression line intersecting all TIC centers.
(4) Recalculate target image pixel values based on the normalization regression function. After this step, the target image and the base image will have been normalized to a common scale.

It should be noted that most previous studies (e.g. Elvidge et al., 1995; Hall et al., 1991; Schott et al., 1988) normalized two Landsat scenes band-by-band, from whence one could compute normalized NDVI or EVI. Few studies (e.g. Stow et al., 2001, 2003) have cross-calibrated NDVI of two scenes directly without band-by-band normalization. Similarly, in this study, NDVI and EVI were calculated for each scene and the TIC normalization method was performed directly to these vegetation indices. The advantages of this direct normalization of vegetation indices are discussed in Section 4.2.

The ETM+ image collected in 2000 was used as the base image to normalize the other two images collected in 1990 and 2001. In this study, ENVI software (Research Systems Inc., Boulder, CO) was used for image processing and ArcMap software (ESRI Inc., Redlands, CA) was used to create the scatter plots and point density maps. To demonstrate the normalization process, we show an example of NDVI normalization of the 2000 image (designated as the base image) and the 2001 image (designated as the target image) in Fig. 4. The x- and y-axes of the scatter plot (Fig. 4a) represent the NDVI values of all collocated pixels in the two subset images of 2000 and 2001 in Fig. 3. The sediments and surface vegetation changes caused negative NDVI in a few water pixels; these pixels were thus excluded in the scatter plot. An NDVI point density map (Fig. 4b) was created based on the scatter plot, with different grayscales used to represent changes in the density of the pixel points at a certain location of the density map. To facilitate identification of TIC centers, the steps of the density scale are unevenly distributed. In this density map example, four local cluster centers were found and the pixels within these cluster centers were selected and relocated on the original Landsat 7 images and high resolution IKONOS image using pixel geographic attributes. Using information from field inventory data and the satellite images, these local cluster centers were interpreted as water, cities/bare lands, conifer/deciduous forests, grass/crop lands, and clouds (Fig. 4b). The first two features have been generally accepted as invariant surface features in previous studies (e.g. Elvidge et al., 1995; Schott et al., 1988). Water is considered as an invariant feature because it contains much lower and more stable reflectance compared to other surface features. Cities (e.g. road surfaces and rooftops) and bare lands (e.g. rocks) are also commonly used as invariant features in previous research because they typically display the brightest invariant pixels and their reflectance vary less than other features in different seasons.

Each temporally invariant cluster (TIC) center was identified as the highest density center of each (pseudo)invariant feature. In this case (using the NDVI density map of 2000 and 2001; Fig. 4b), the TIC centers of water and cities/bare lands defined a normalization regression line. The cluster centers of conifer/deciduous forests and grass/crop lands were slightly lower than the linear regression line due to seasonally-induced phenological differences of the vegetation between the two observation dates. This also

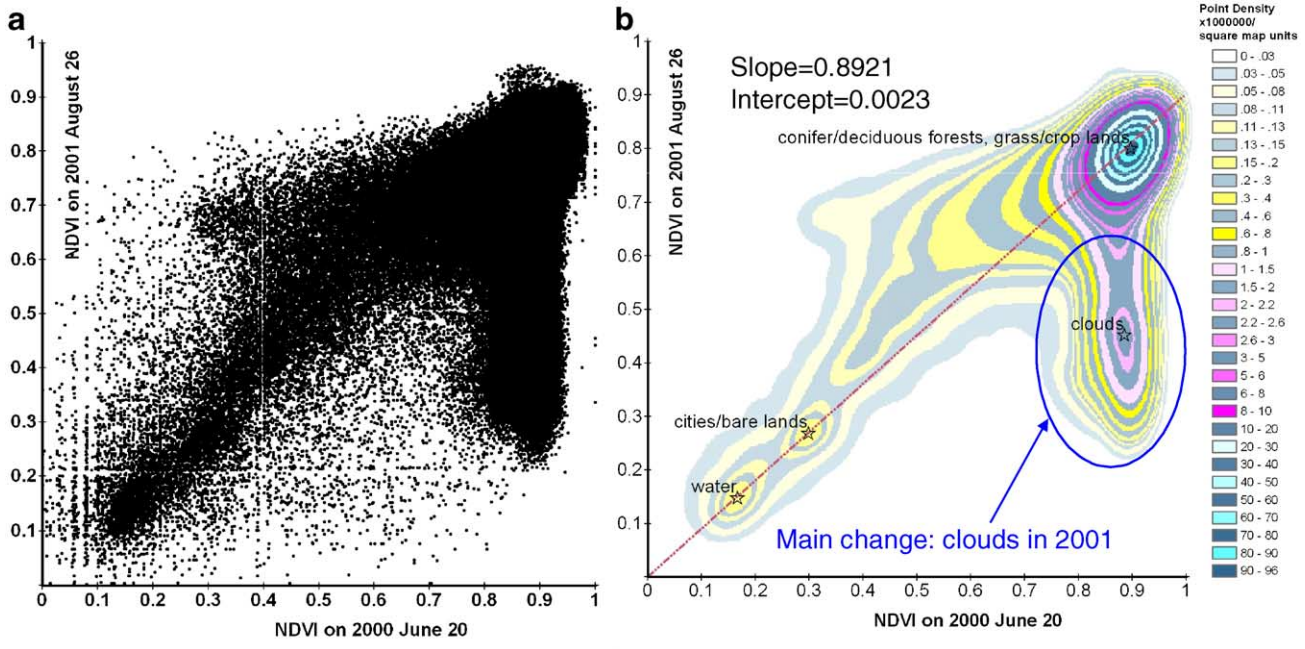

Fig. 4. NDVI scatter plot (a) and point density map (b) of 2000 vs. 2001 ETM+ images prior to normalization. A normalization regression line was created through two TIC centers: water and cites/bare lands (slope=0.8921, intercept=0.0023).

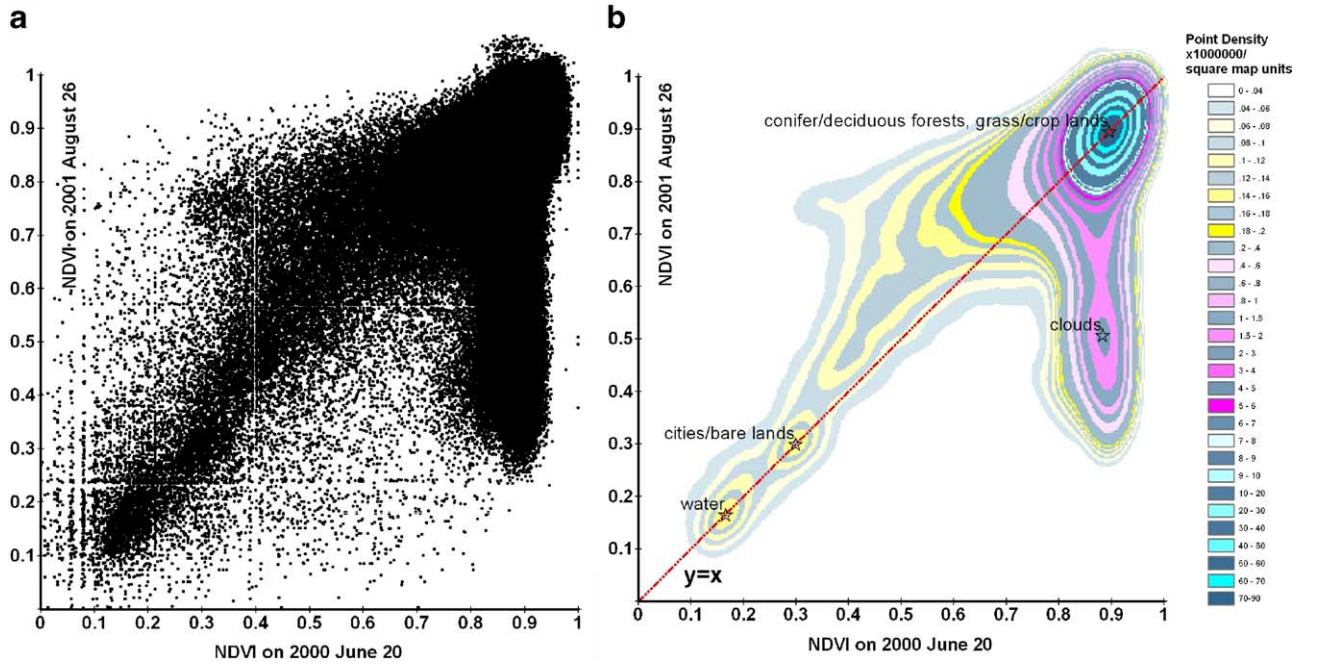

Fig. 5. NDVI scatter plot (a) and point density map (b) of 2000 vs. 2001 ETM+ images after normalization.

confirmed the assumption that the radiometric correlation of NDVI is linear across the two observations. The regression function with a slope of 0.8921 and an intercept of 0.0023 was used to recalculate the 2001 target image. Thus, after the normalization, the NDVI values for 2001 were changed to the new (normalized) scatter plot and density map shown in Fig. 5. After the normalization, most pixel values were very close to the $x=y$ regression line, demonstrating that the two images shared a common scale and could be quantitatively compared in further study. Pixels located away from the regression line contained spectral variation through time, upon which further analysis was based.

3. Results

3.1. Radiometric normalization of vegetation indices

Landsat 7 ETM+ (2000, 2001) and Landsat 4 TM (1990) data were used for NDVI normalization study (Figs. 4–6). Because NDVI exhibited a small range of values for vegetated surfaces, all vegetation pixels clustered closely to form one mixed cluster center (Figs. 4–6). In the NDVI density maps, regression lines were created to intersect the two TIC centers (water, cities/bare lands); the cluster center of mixed vegetation fell slightly off the regression line due to seasonal changes in vegetation. The cloud pixels in the 2001 image contained significantly lower NDVI values than the vegetation pixels in 2000, thus they formed a cluster center in the density map (Fig. 5b). The shaded vegetation pixels in 2001 had very similar NDVI values to those in 2000 and occurred close to the mixed cluster center and the normalization regression line. Thus shaded vegetation could not be distinguished from sunlit vegetation using the density map. This finding demonstrates that NDVI is a good index to reduce illumination influences and extract vegetation information under shadow. In the NDVI density map of 2000 vs. 1990 (Fig. 6) the water cluster exhibited a lower density than what was found when comparing 2000 vs. 2001 imagery (Fig. 4b). This indicates that the channel of the river shifted over a period of ten years due to geomorphological and other processes. Another likely reason for the scattering of water pixels might be due to the resampling of the 1990 image. The 28.5-m resolution from the 1990 image did not completely match the 30-m resolution from the 2000 image, and after the resampling, the pixel values of the 1990 image might have slightly changed. However, though some water pixels changed during the 10-year period and the local cluster center of water was small, manual inspection of those center pixels indicated that they were spectrally invariant over time and the resulting low density cluster was considered as a TIC center. The landcover changes in urban and vegetation were also detected in the NDVI density map of 2000 vs. 1990 (Fig. 6). After normalization, these pixels contained significantly higher NDVI values in 2000 than in 1990. However, it was difficult to specify the type of landscape change, based on the fact that the ability to distinguish among forests, crops, and grasslands was difficult using NDVI.

Although NDVI was not useful in distinguishing among vegetation types at this location, coniferous forests did exhibit some substantially different reflectance properties from deciduous forests and grass/crop lands as a result of different canopy structure. Thus, EVI values of vegetated pixels exhibited a larger dynamic range than did NDVI. TIC centers of water and cities/bare lands defined a normalization regression line that also bisected the cluster center of high

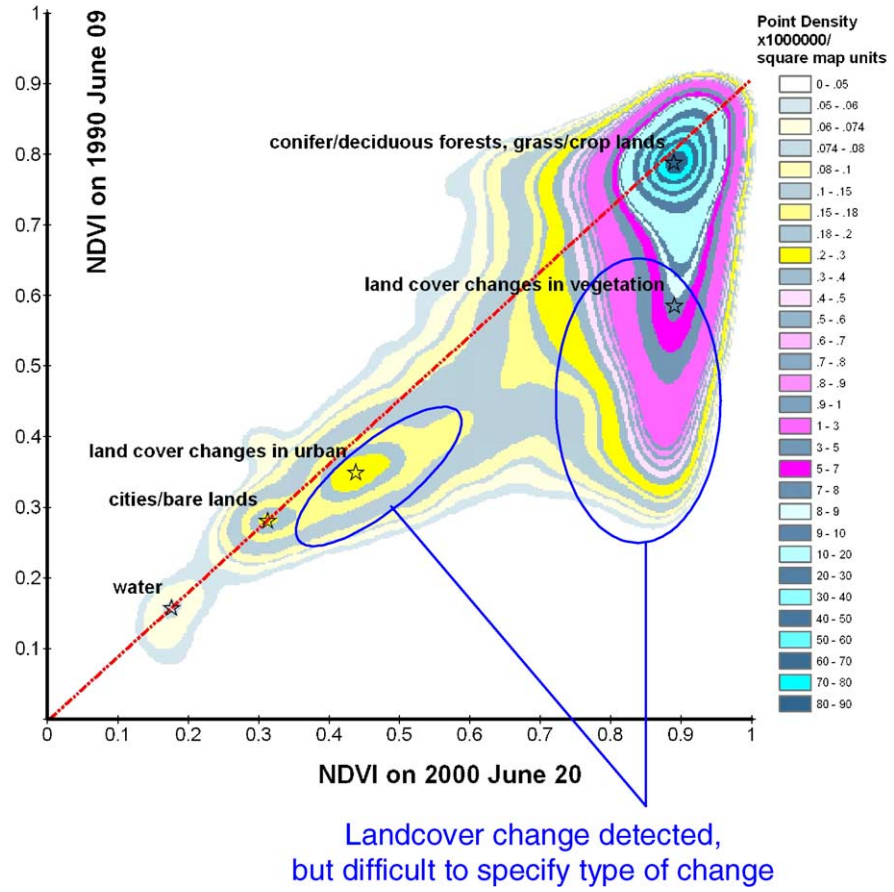

Fig. 6. NDVI point density map of 2000 Landsat 7 vs. 1990 Landsat 4 data.

density coniferous forests (Fig. 7a). The high density coniferous forests were the dominant surface covers in the study subset, and field measurements indicate that in some of these pixels the LAI values are higher than 8 (A. Conley et al., unpublished data). In these high density coniferous forests, the reflectance of the dense evergreen overstory changed little through time. Thus, although two TIC centers had already been identified, the high density coniferous forest was also considered to be a TIC center in this case due to its invariant spectra in multiple observations. The fact that the linear regression line intersected three distinct TIC centers also confirmed the assumption that the radiometric correlation of EVI was linear across the two observations. The regression function (slope=0.7715; intercept=0.0089) was used to recalculate the target (2001) image (Fig. 7a). After the normalization, the EVI values of 2001 were recalculated, with the new density map shown in Fig. 7b. After normalization, most pixel values were very close to the $x=y$ regression line, demonstrating that the two images shared a common scale and could be quantitatively compared.

Upon normalization, two types of surface change could be readily identified using the EVI density map of images collected in 2000 vs. 2001 (Fig. 7b). One surface feature involved vegetation pixels occurring in the cloud shadow. Fig. 7b-1 shows the range of pixels influenced by cloud shadows in 2001. These pixels had higher EVI values in 2000 under clear skies than in 2001 when shadowed. Through the geographic attributes of these pixels, we identified two surface features as shadowed conifer forests and shadowed deciduous forests in 2001. Another pixel cluster center under cloud shadow was likely mixed deciduous–conifer forests, with EVI values occurring between those of the above two features. The mixture center of deciduous forests and grass/crop lands contained very high EVI values compared with the other cluster centers (Fig. 7b-2). The EVI values of mixed forests likely fell between the conifer forest TIC center and the deciduous forests and crop/grass lands cluster center, helping to define a high density ridge of vegetation pixels in the point density map. This ridge was slightly different from the TIC normalization regression line due to real differences in vegetation phenology and density between the image dates; most non-conifer vegetation pixels had higher EVI values in the mid summer (June 20) than late in the growing season (August 26). Comparisons between the vegetation under cloud shadow and the vegetation under clear sky reveal that the deciduous forests shadowed by the cloud exhibited similar EVI values to unshadowed conifer forests (Fig. 7b). This finding demonstrates that EVI is very sensitive to shadowing influences and explains why EVI can produce

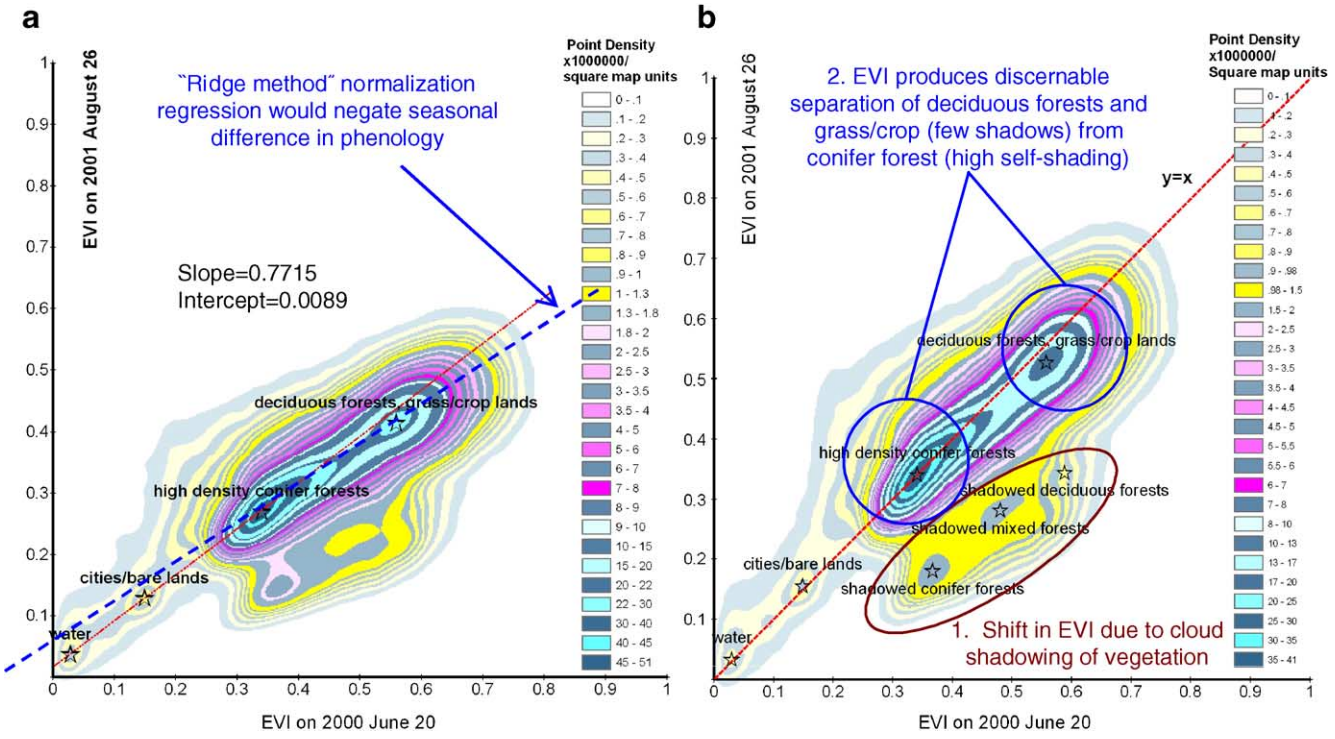

Fig. 7. EVI point density maps of 2000 vs. 2001 ETM+ images before normalization (a) and after normalization (b).

discernable separation of deciduous forests and crop/grass lands (containing relatively few shadows) from conifer forests (containing high amounts of self-shading). The cloud pixels in 2001 contained EVI values similar to those mixed forests and were therefore mixed in the high density ridge. Thus, the cloud could not be separated from other features in the EVI density map.

In the EVI density map of 2000 vs. 1990 images (Fig. 8), cities/bare lands and high density conifer forests were again considered as TIC centers based on their stable reflectance across dates. The water cluster center was smaller than that of 2000 vs. 2001 shown in Fig. 7a. Some water pixels exhibited changed EVI values due to image resampling and natural surface changes, thus it formed a cluster center below the normalization regression line created by the above two TIC centers. The regression line also went through some invariant water pixels, though they did not form a cluster center because they were close to the other variant water pixels (Fig. 8). In the density map, land cover change due to conifer deforestation could be readily identified (Fig. 8). Deforested pixels exhibited low EVI values in 1990 (analogous to conifer forests) and high EVI values in 2000 (showing their new status as crop/grass lands). In addition, the high density ridge of vegetation was slightly above the regression line and indicated that after the normalization, non-conifer vegetation pixels contained higher EVI values earlier in the short Siberian growing season (June 9 vs. June 20).

A point density map of Reduced Simple Ratio (RSR) is shown in Fig. 9. In this map, the base image was again from 2000 and the target image was from 2001. The cloud pixels from 2001 exhibited negative RSR values whereas in 2000 they had exhibited high RSR values as clear vegetation pixels. The vegetation under cloud shadows in 2001 contained similar RSR values to the coniferous forests and could not be separated in the density map. Water pixels occurred close to the cities/bare lands cluster center, thus for RSR water pixels did not form a separate cluster center. Most water and cities/bare lands pixels contained negative RSR values. The high density conifer forest cluster center contained much higher RSR values compared to the deciduous forests and grass/crop lands cluster center. The high density ridge of the vegetation in the RSR density map was obviously nonlinear, and the TIC method could therefore not be used to normalize the RSR directly. Band-by-band normalization must be done before calculating the RSR for the target image. The reasons of the nonlinear correlation of RSR in two observations were likely due to the nonlinearity of the RSR calculation (Eq. (5)) and also due to the sensitivity of shortwave infrared (SWIR) radiance to vegetation acquired on different dates.

3.2. Improvement of surface LAI monitoring

As a test of normalization efficacy, EVI and NDVI images were compared with field LAI data collected in 2000 and 2001 at two conifer forest sites. Prior to normalization, the data points collected in 2001 (grey diamond points) were noticeably incongruous with data points collected in 2000

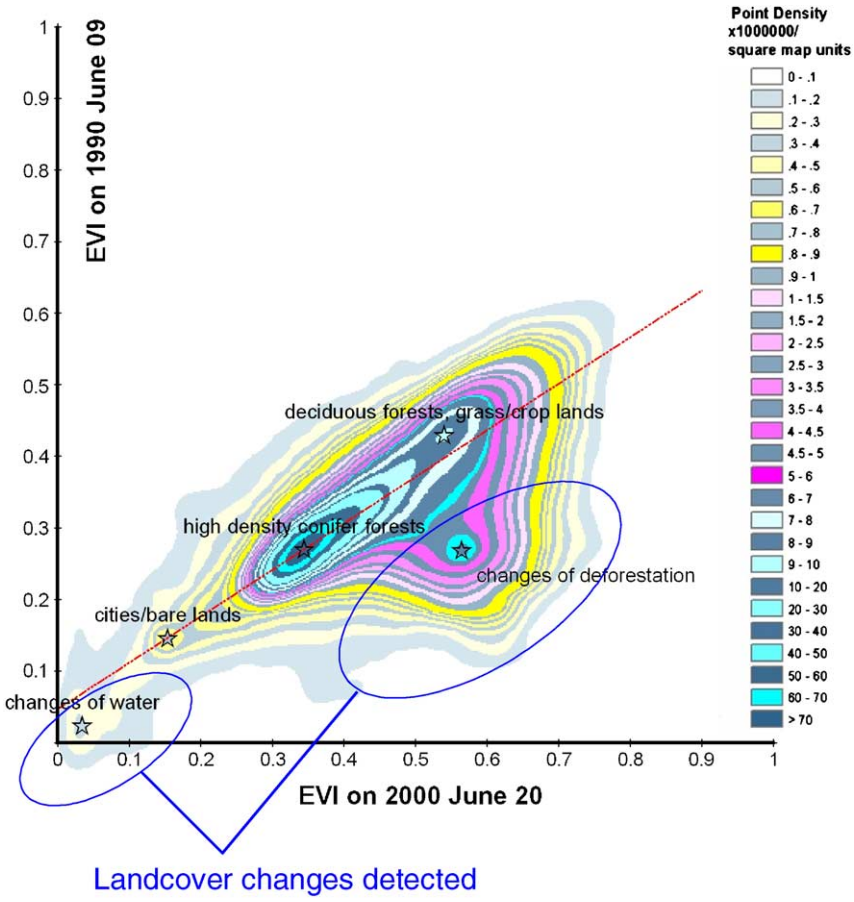

Fig. 8. EVI point density map of 2000 Landsat 7 vs. 1990 Landsat 4 data. Note that land cover changes between these periods can be quantified as a shift from conifer forests to deciduous forest and/or grass/crop lands using the EVI.

(Figs. 10 and 11). After the normalization, these data values increased and fit into those data points collected in 2000. Therefore, as a result of normalization, the r^2 value of the EVI-LAI logarithmic regression function significantly improved, from 0.46 to 0.61 (Fig. 10). Similarly, the r^2 value of NDVI-LAI linear regression function improved from 0.49 to 0.69 (Fig. 11). These results demonstrate that the TIC method can be used to successfully normalize satellite data to a common radiometric scale and provide consistent, reliable, and comparable information.

Although EVI was more useful for separating vegetation cover types than NDVI (Figs. 7 and 8), the LAI correlation was poorer for EVI ($r^2=0.61$) than for NDVI ($r^2=0.69$). The likely reason for this result is the summertime "cancellation effect" of EVI in mixed conifer–grass pixels. Chen et al. (2004, 2005) found that EVI was negatively correlated with the conifer tree/shade area fraction within satellite image pixels, but positively correlated with the grass area fraction when images were collected during the period of summertime understory greenness. According to the post-fire LAI dynamics seen in field collected data (Fig. 12), the understory (grass and forbs) LAI increased significantly during the first few years after fire and decreased when the overstory (trees) started to recover. The total combination of overstory and understory led to changing correlations between total LAI and EVI in different post-fire ages. This "cancellation effect" was demonstrated in our conifer study sites. The slopes of the EVI-LAI correlation functions changed from positive to negative due to the various overstory and understory contribution in different post-fire ages (Fig. 13) and corroborates similar findings in a North American ponderosa pine forest canopy (Chen et al., 2004, 2005).

3.3. Vegetation monitoring across a fire chronosequence

We investigated Siberian pre/post-fire vegetation dynamics using the normalized EVI and NDVI Landsat images from 1990, 2000, and 2001 (Fig. 14). The cloud-influenced 2001 deciduous forest data (Fig. 3) were excluded in this dynamic analysis. Because it is not known what vegetation types occurred in 1990 at the mid-successional deciduous forest sites, these sites are denoted as "unknown" vegetation in Fig. 14. NDVI values of conifer forest sites were substantially reduced during the first two years post-fire (Fig. 14a), owing to the fact that NDVI was sensitive to the soil background changes after fire. Coniferous forests exhibited similar EVI values before and after fire, (Fig.

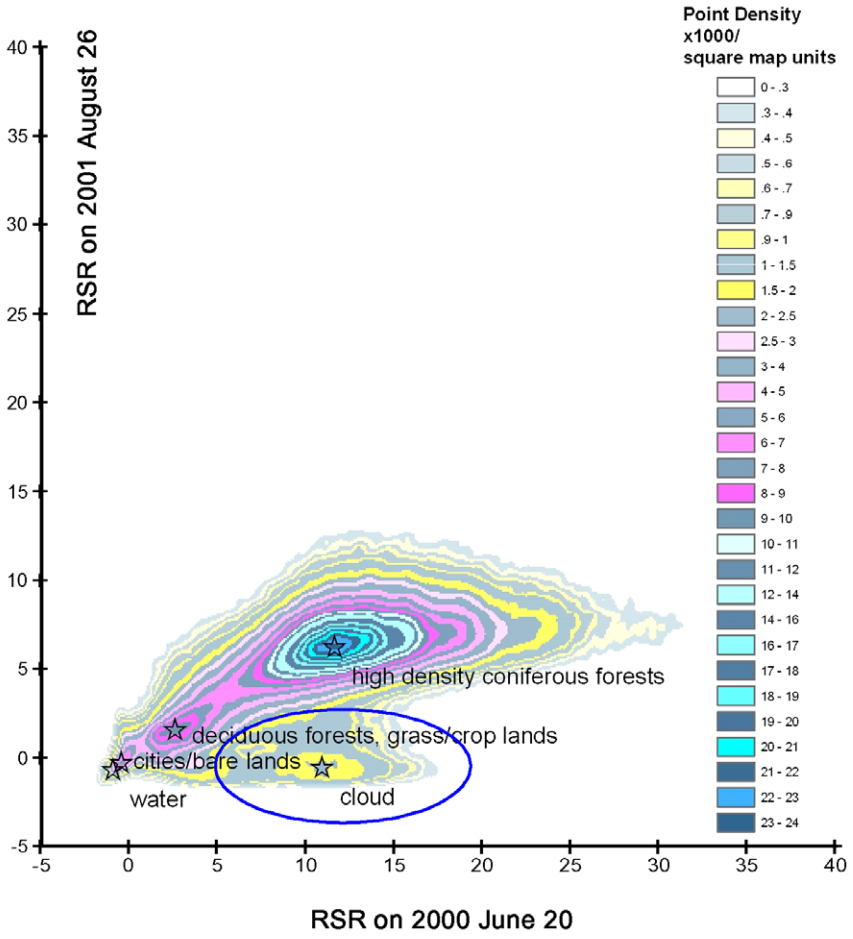

Fig. 9. RSR point density map of 2000 vs. 2001 ETM+ images. The clouds in image 2001 are highlighted by the oval.

14b) with a difference <0.05. This was likely due to the "cancellation effect" of EVI in coniferous forests (Chen et al., 2004, 2005): EVI values remain relatively stable when high density conifer overstory is replaced by intermediate density understory after fire. We also found that most EVI values of deciduous forests were significantly higher than EVI of conifer forests, while their NDVI values were similar and difficult to separate. EVI also contained a larger range of values for all study plots (0.44) than did NDVI (0.39). This further indicates that EVI was more sensitive to canopy structure and had the capability to separate coniferous forests from deciduous forests.

3.4. Comparison of the TIC method to other relative radiometric normalization methods

The TIC method not only contains point density statistics of pixels in the scenes, but also enables the original images to be combined with ancillary information to interpret the cluster centers. The temporally invariant cluster method is

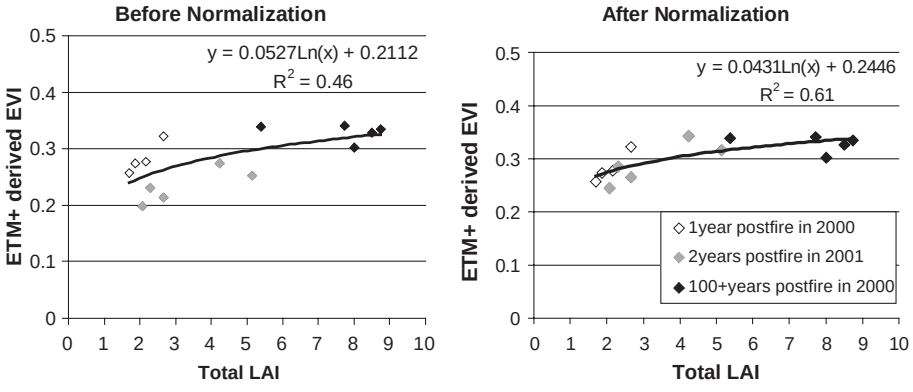

Fig. 10. Comparison of total field-measured LAI with EVI derived from conifer forest in 2000 and 2001 ETM+ images.

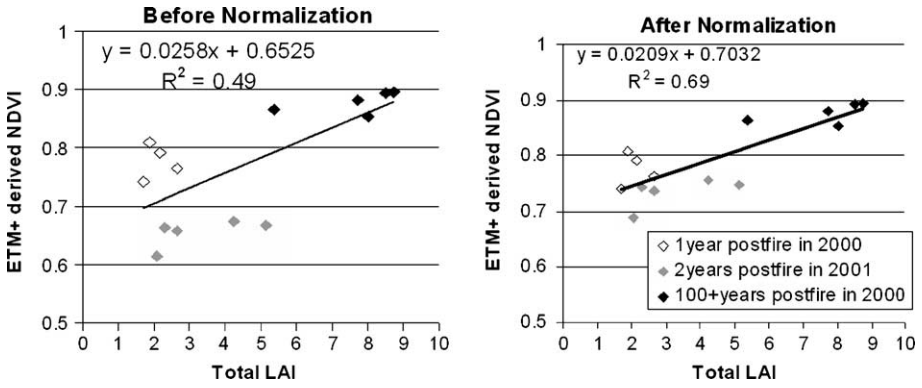

Fig. 11. Comparison of total field-measured LAI with NDVI derived from conifer forest in 2000 and 2001 ETM+ images.

simple yet effective. It can be used to normalize band-specific reflectance or raw digital number (DN; analyses not shown), or can normalize linearly correlated vegetation indices (such as NDVI and EVI in this study) as long as the image data satisfies the aforementioned assumptions.

Our initial development of the TIC method was a response to the fact that we encountered some problems and limitations when using some previous relative radiometric correction methods in this study subset. The TIC method normalized atmospheric effects (including path and scattering influences), satellite sensor noise, and differences of solar angle and view angle in one calculation step, while the dark objective subtraction (DOS) could only reduce the scattering influence and the combination result of two scenes was not satisfactory (data not shown). Although the selection of invariant pixels and creation of regression functions in the TIC method are conceptually similar to pseudoinvariant features (PIF) techniques, in previous PIF work spectrally pseudoinvariant features are required to represent a majority of the image area in order to conduct successful normalization (e.g. Du et al., 2002; Elvidge et al., 1995). In this study, we analyzed histogram statistics, principal components, and the Kauth–Thomas (KT) greenness–brightness scattergram (Du et al., 2002; Elvidge et al., 1995; Hall et al., 1991; Schott et al., 1988) to identify PIFs following established methods. However, visual inspection of the images demonstrated that these PIFs contained intractable errors because the subset (also the whole scene) contained many fewer pseudoinvariant pixels (e.g. water, bare soil/cities) than the variant vegetation pixels due to seasonal and land use changes. In contrast, the TIC method only requires that invariant features have distinguishable spectral characteristics so that there are at least two TIC centers to create a regression function, regardless of the absolute number of temporally invariant pixels. Because the normalization regression function is based on the highest local density centers of the temporally invariant pixels, the variant pixels do not influence the regression line. These advantages indicate that the TIC method can provide a more accurate regression line compared to previous radiometric normalization when temporally variant pixels (e.g. vegetation) predominate.

Though both the TIC method and the ridge method utilize the point density map to create a regression line to normalize the target image, these two methods contain significant differences. The ridge method assumes that most pixels of the scene are spectrally invariant and that the normalization regression line follows the high density ridge, while the TIC method uses the temporally invariant cluster (TIC) centers to define the regression line (e.g. Fig. 4) with no requirement that most pixels are invariant. Thus, the TIC centers do not need to contain high densities of pixels; rather, they can be low density pixel clusters as long as they can be distinguished from other features. In the NDVI normalization example, <5% of the pixels in the subset images contained

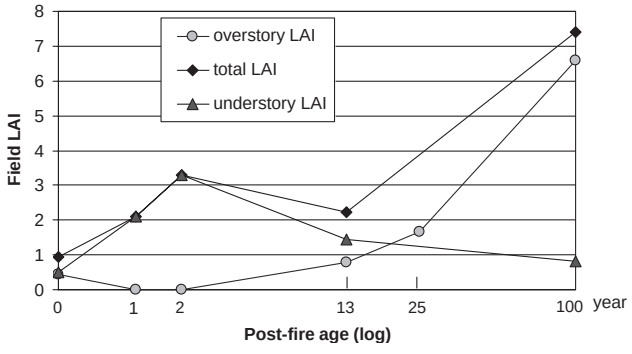

Fig. 12. Post-fire LAI dynamics based on field measures in 1999, 2000, and 2001 summer time (according to the data in the study of Deering et al., in preparation).

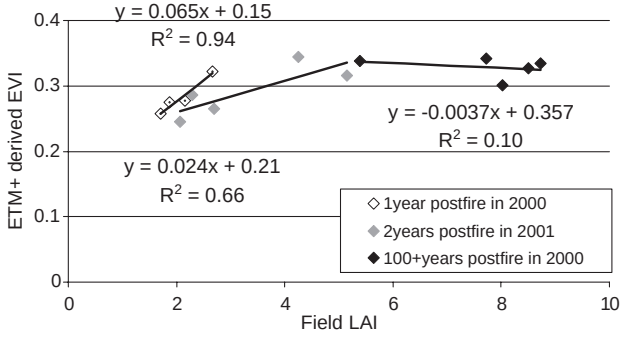

Fig. 13. "Cancellation effect" of EVI vs. LAI as manifest across post-fire chronosequence.

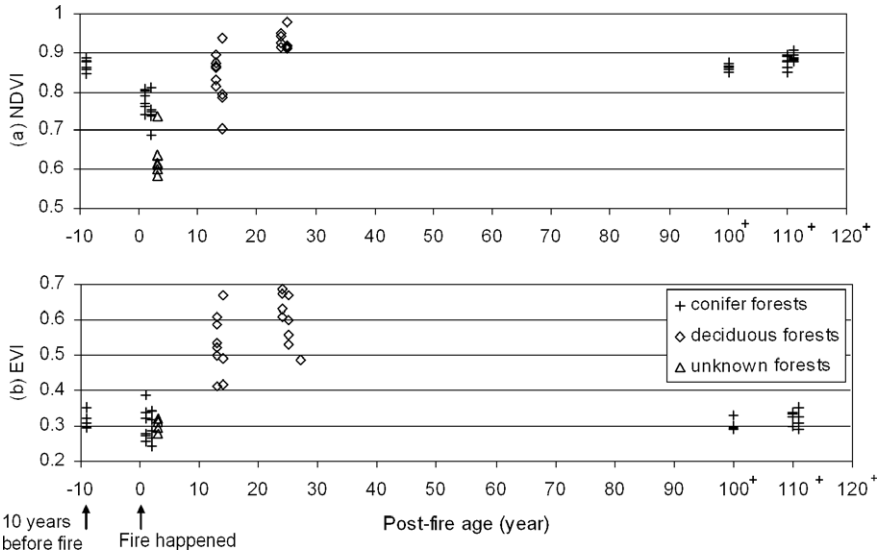

Fig. 14. Siberian pre/post-fire NDVI (a) and EVI (b) dynamics of field plots using normalized Landsat 4 (1990) and Landsat 7 (2000 and 2001) images.

pseudoinvariant features (i.e. water and cities/bare lands) and >80% of the pixels were dominated by vegetation cover. The normalization regression line intersects two TIC centers (water and cities/bare lands) in the NDVI density map (Fig. 4b). However, the pixels representing clouds and mixed vegetation would have defined an erroneous near-vertical "high density ridge" had we employed the ridge method for the normalization (Fig. 4b). Excluding the cloud pixels, the high density vegetation pixels clustered to form one center without a significant ridge. Alternatively, EVI is sensitive to various vegetation types and therefore the vegetation pixels do form a high density ridge in the EVI density map. If a ridge method were used to create a regression line, it would resemble the dashed line in Fig. 7a, following the high density ridge of vegetation pixels. This ridge regression line would not cross the invariant features of water or cities/bare lands due to ridge distortion caused by vegetation phenological and/or growth differences between the June and August images of different years. In investigating band-by-band reflectance density plots of ETM+ 2000 vs. 2001 imagery, we found that the "no ridge" situation occurred in the blue band, and the "phenologically distorted ridge" occurred in the other five optical bands. By preferentially weighting the low density TIC centers, the regression line defined by the TIC method can preserve sensitivity to phenological differences that would have been obscured or negated by selecting a normalization line to follow the high density ridge.

4. Discussion and conclusions

4.1. Temporally Invariant Cluster (TIC) method

Based on the assumptions of the temporally invariant cluster (TIC) method, at least two TIC centers were extracted from the point density maps defined by each base/target image pair. Selection of these TIC centers is not automatic, but rather is based upon observation of the point density map in conjunction with visual examination of the original images to confirm that those pixels located at the TIC centers are truly spectrally invariant. A regression line is established through these TIC centers, which defines the normalization function used to recalculate the target image such that it contains a common radiometric scale with the base image. The TIC method therefore not only utilizes statistical analysis (point density statistics) of the pixels in the scenes, but also can be used in combination with the original images and other ancillary information to interpret the cluster centers. This method may not only be used to normalize the general reflectance or raw digital number (DN) at each specific band (analyses not shown), but also be used to normalize linearly correlated vegetation indices (NDVI and EVI, this study) as long as the image data satisfy the assumptions.

In very rare cases, the images to be normalized may consist entirely of variant pixels, or the invariant surface features will not exhibit clearly distinct spectral properties. In these cases, invariant pixels could be manually selected to create a point density map. In this way, the normalization regression line could still be created, but would contain a certain degree of subjective influence.

Though large efforts have been made to interpret forest structure parameters, such as LAI, from remotely sensed data, few studies have used multi-temporal satellite data and field LAI data to interpret the correlation. In this study, the TIC method was used to normalize Landsat 4 TM 1990 image and Landsat 7 ETM+ 2001 image based on the ETM+ 2000 base image acquired for Siberian study sites. After the normalization, the field LAI correlation (r^2) with EVI and NDVI showed substantial improvement from 0.46 to 0.61 and from 0.49 to 0.69, respectively (Figs. 10 and

11). In addition, the TIC method greatly benefited the analysis of post-fire dynamics using 1990, 2000, and 2001 Landsat images to trace the changes of vegetation indices in conifer and deciduous forests along a fire chronosequence (Fig. 14).

Different radiometric correction algorithms have various advantages and disadvantages so that no single method can be used in all situations (Lu et al., 2004). Compared to some previous relative radiometric normalization methods, however, this new TIC method offers several improvements and advantages. The new method can avoid the influence of variant pixels by using a point density map to identify TIC centers and therefore avoid undue influences of variant pixel cluster centers. In addition, the method is very simple and technically straightforward and does not require advanced programming and statistical skills (e.g. Chavez, 1996). The TIC method can outperform DOS methods to normalize atmospheric effects, satellite sensor noise, and differences of solar angle and view angle in one step without extra in situ parameters. Though large expanses of variant vegetation cover and density ridge distortion of multi-seasonal images can limit the utility of several previous PIF methods and the ridge method in detecting change across the landscape, TIC centers are formed by high local density (though not necessarily high absolute density) clusters of invariant pixels and are not influenced by the variant pixels. Compared to the ridge method (Song et al., 2001), the TIC method can separate pixels influenced by phenological and anthropogenic change from the pixels upon which normalization is based, thereby increasing the likelihood that subtle changes can be detected rather than "normalized away". We note, however, that the selection of the most effective radiometric normalization approach for a given application must be based on the specific project objective, the study location, and the available ancillary data. We found the TIC method to be indispensable in normalizing images (where few invariant pixels existed) to remotely study post-fire LAI and other land cover change in this boreal ecoregion. Additional work is necessary, however, to compare the TIC method with other normalization methods in other study areas under a range of study objectives.

4.2. Vegetation indices and their use in image normalization

In previous studies, images are typically normalized band-by-band before calculating vegetation indices (e.g. Du et al., 2002). Though a thorough comparison of band-by-band vs. VI-based normalizations is beyond the scope of this study due to the lack of in situ atmospheric measurements, we have found three advantages of directly normalizing vegetation indices. First, vegetation indices are designed to combine spectral information from multiple bands so as to more effectively relate to surface changes than individual bands (Coppin et al., 2004). Therefore, scattergrams derived from vegetation indices can better represent changes in vegetation and therefore are more intuitive for correctly identifying TIC centers. Second, direct normalization of vegetation indices can reduce data volume for normalization processing and analysis. For example, band-by-band techniques require that the normalization be conducted separately on three bands (blue, red, and NIR) before calculating the EVI with the normalized data, whereas a direct normalization only requires the calculation of EVI prior to a one step normalization process. The direct method can create efficiencies especially for large data sets and large study regions. A third advantage is that the direct normalization of VIs can reduce error compared to traditional band-by-band methods, because errors accumulate when using separately-normalized bands for VI calculations.

In this study the newly developed TIC method was used to normalize NDVI and EVI of multi-temporal Landsat 4 TM and ETM+ images directly. The linear regression lines intersecting the TIC centers in point density maps of NDVI and EVI confirmed the assumption that radiometric correlations of these two vegetation indices were linear during the multiple observations (Figs. 4 and 7). Similar results were reported by Myneni and Asrar (1994). This important finding can greatly benefit future study using relative radiometric correction methods on vegetation indices. The nonlinear radiometric correlation of RSR due to atmospheric effects was also demonstrated in this study using a point density map of two observations in 2000 and 2001 (Fig. 9).

Both NDVI and EVI are important vegetation indices for landscape change detection. Previous study has demonstrated that NDVI was sensitive to soil background (e.g. Elvidge & Lyon, 1985; Huete et al., 1985), while EVI was more responsive to canopy structure as EVI contains the correction of canopy background and atmospheric scattering influences (Gao et al., 2000). In this study, EVI values of crop/grass lands and deciduous forests were significantly higher than coniferous forests, while their NDVI values were very close and difficult to separate (Figs. 4, 7 and 14). EVI also exhibited a large range of values for vegetation surfaces and formed a high density ridge in the density map. Unlike EVI, the range of NDVI values was much smaller and there was only one mixed cluster comprised of vegetation pixels of all types.

Analyses of shadow influences demonstrate that EVI is very sensitive to cloud shadows, as the EVI values of vegetation under a cloud shadow decreased significantly. This sensitivity to shadowing could be a reason for the EVI sensitivities of various canopy structures containing different levels of self-shadowing. In the NDVI density map, the vegetation under shadow contained similar values as the vegetation in sunlight. This indicated that NDVI was a very effective vegetation index to reduce the variability due to shadowing influences yet retain vegetation-related information (Sabol et al., 2002). In addition, NDVI was also good at capturing the changes of post-fire in coniferous forests due to its sensitivity to soil backgrounds (Fig. 14) (Elvidge & Lyon, 1985; Huete et al., 1985).

4.3. EVI "cancellation effect"

Previous work has found that a positive correlation exists between the EVI and understory grass cover fraction, yet a negative correlation exits between the EVI and overstory conifer tree cover fraction during peak summertime greenness (Chen et al., 2004). This caused a "cancellation effect" in relating the EVI to overall ecosystem LAI in various post-fire age conifer forests. Analysis of field data collected across a fire chronosequence quantified the LAI dynamics of the overstory and understory (Fig. 12) in these Siberian boreal forests. With the increase of the post-fire age, the overstory increased significantly to a local peak and then decreased when the overstory became dominant. In our coniferous forest study sites, the multi-temporally-collected image data and field data were used to interpret the "cancellation effect". The slope of correlation function of EVI and field LAI changed from positive to negative when the post-fire age of study sites increased (Fig. 13). This EVI "cancellation effect" can degrade the strength of the EVI–LAI relationship for mixed pixels in conifer systems.

Although this study has focused upon a subset in Siberian boreal forests, the TIC method is likely to be effective for analyzing satellite images across a wide range of terrestrial ecosystems and warrants further use. The above findings indicate that the TIC method provides a simple, effective and repeatable method to improve change detection using satellite images across sensors and/or across time.

Acknowledgements

This research was supported by NASA EPSCoR grant NCC5-588 and NSF grant DBI-9985039. We would like to acknowledge the Terrestrial Ecology Program of the NASA Earth Science Enterprise for funding the field research in Siberia. We thank Alexis Conley and Anastassia Nelzina for coordinating the field studies in Siberia, and William Capehart for his comments on an earlier draft of the paper. We appreciate two anonymous reviewers providing comments on an earlier version of this manuscript.

References

Andrefouet, S., Muller-Karger, F. E., Hochberg, E. J., Hu, C., & Carder, K. L. (2001). Change detection in shallow coral reef environments using Landsat 7 ETM+ data. *Remote Sensing of Environment*, *78*, 150–162.

Brown, L. J., Chen, J. M., Leblanc, S. G., & Cihlar, J. (2000). Short wave infrared correction to the simple ratio: an image and model analysis. *Remote Sensing of Environment*, *71*, 16–25.

Chavez, P. S. (1996). Image-based atmospheric corrections—Revisited and improved. *Photogrammetric Engineering and Remote Sensing*, *62*, 1025–1036.

Chen, J. M., & Cihlar, J. (1996). Retrieving leaf area index of boreal conifer forest using Landsat TM images. *Remote Sensing of Environment*, *55*, 153–162.

Chen, J. M., Pavlic, G., Brown, L., Cihlar, J., Leblanc, S. G., & White, H. P., et al. (2002). Derivation and validation of Canada-wide coarse-resolution leaf area index maps using high-resolution satellite imagery and ground measurements. *Remote Sensing of Environment*, *80*, 165–184.

Chen, X., Vierling, L., Rowell, E., & DeFelice, T. (2004). Using lidar and effective LAI data to evaluate IKONOS and Landsat 7 ETM+ vegetation cover estimates in a ponderosa pine forest. *Remote Sensing of Environment*, *91*, 14–26.

Chen, X., Vierling, L., Deering, D., & Conley, A. (2005). Monitoring boreal forest LAI across a Siberian burn chronosequence: A MODIS validation study. *International Journal of Remote Sensing,* in press.

Cohen, W. B., Maiersperger, T. K., Gower, S. T., & Turner, D. P. (2003a). An improved strategy for regression of biophysical variables and Landsat ETM+ data. *Remote Sensing of Environment*, *84*, 561–571.

Cohen, W. B., Maiersperger, T. K., Yang, Z., Gower, S. T., Tumer, D. P., & Ritts, W. D., et al. (2003b). Comparisons of land cover and LAI estimates derived from ETM+ and MODIS for four sites in North America: A quality assessment of 2000/2001 provisional MODIS products. *Remote Sensing of Environment*, *88*, 233–255.

Coppin, P., Jonckheere, I., Nackaerts, K., Muys, B., & Lambin, E. (2004). Digital change detection methods in ecosystem monitoring: A review. *International Journal of Remote Sensing*, *10*, 1565–1596.

Deering, D. W., Conley, A. H., Nelzina, A. G., Kharuk, V. I., Leblanc, S. G., Kofman, G. B., Chen, J. M., and Vierling, L. A. (in preparation). Leaf area index across post-fire Siberian boreal forests. *Canadian Journal of Forest Research*.

Du, Y., Teillet, P. M., & Cihlar, J. (2002). Radiometric normalization of multitemporal high-resolution satellite images with quality control for land cover change detection. *Remote Sensing of Environment*, *82*, 123–134.

Elvidge, C. D., & Lyon, R. J. P. (1985). Influence of rock–soil spectral variation on the assessment of green biomass. *Remote Sensing of Environment*, *17*, 265–279.

Elvidge, C. D., Yuan, D., Weerackoon, R. D., & Lunetta, R. S. (1995). Relative radiometric normalization of Landsat Multispectral Scanner (MSS) data using an automatic scattergram-controlled regression. *Photogrammetric Engineering and Remote Sensing*, *61*, 1255–251260.

Gao, X., Huete, A. R., Ni, W., & Miura, T. (2000). Optical–biophysical relationships of vegetation spectra without background contamination. *Remote Sensing of Environment*, *74*, 609–620.

Hall, F. G., Strebel, D. E., Nickeson, J. E., & Geoets, S. J. (1991). Radiometric rectification: Toward a common radiometric response among multidate, multisensor images. *Remote Sensing of Environment*, *35*, 11–27.

Huete, A., Didan, K., Miura, T., Rodriguez, E. P., Gao, X., & Ferreira, L. G. (2002). Overview of the radiometric and biophysical performance of the MODIS vegetation indices. *Remote Sensing of Environment*, *83*, 195–213.

Huete, A. R., Jackson, R. D., & Post, D. F. (1985). Spectral response of a plant canopy with different soil backgrounds. *Remote Sensing of Environment*, *17*, 37–53.

Huete, A. R., Liu, H. Q., Batchily, K., & Leeuwen, V. W. (1997). A comparison of vegetation indices over a global set of TM images for EOS-MODIS. *Remote Sensing of Environment*, *59*, 440–451.

Kaufman, Y. J. (1988). Atmospheric effect on spectral signature. *IEEE Transactions on Geoscience and Remote Sensing*, *26*, 441–451.

Lillesand, T. M., & Kiefer, R. W. (1994). *Remote sensing and image interpretation*. John Wiley and Sons.

Lu, D., Mausel, P., Brondizio, E., & Moran, E. (2004). Change detection techniques. *International Journal of Remote Sensing*, *25*, 2365–2407.

Miura, T., Huete, A. R., Yoshioka, H., & Holben, B. N. (2001). An error and sensitivity analysis of atmospheric resistant vegetation indices derived from dark target-based atmospheric correction. *Remote Sensing of Environment*, *78*, 284–298.

Myneni, R. B., & Asrar, G. (1994). Atmospheric effects and spectral vegetation indices. *Remote Sensing of Environment*, *47*, 390–402.

Myneni, R. B., Keeling, C. D., Tucker, C. J., Asrar, G., & Nemani, R. R. (1997). Increased plant growth in the northern high latitudes from 1981 to 1991. *Nature*, *386*, 698–702.

Roderick, M. L., Noble, I. R., & Cridland, S. W. (1999). Estimating woody and herbaceous vegetation cover from time series satellite observations. *Global Ecology and Biogeography*, *8*, 501–508.

Roughgarden, J., Running, S. W., & Matson, P. A. (1991). What does remote sensing do for ecology? *Ecology*, *72*, 1918–1922.

Rouse, J. W., Haas, R. H., Schell, J. A., & Deering, D. W. (1974). *Monitoring vegetation systems in the Great Plains with ERTS*. Greenbelt: NASA SP-351.

Sabol, D. E., Gillespie, A. R., Adams, J. B., Smith, M. O., & Tucker, C. J. (2002). Structural stage in Pacific northwest forests estimated using simple mixing models of multispectral images. *Remote Sensing of Environment*, *80*, 1–16.

Salvaggio, C. (1993). Radiometric scene normalization utilizing statistically invariant features. *Proceedings of the workshop on atmospheric correction of Landsat imagery* (pp. 155–159).

Schott, J. (1997). *Remote sensing—The image chain approach*. New York: Oxford University Press.

Schott, J. R., Salvaggio, C., & Volchok, W. J. (1988). Radiometric scene normalization using pseudoinvariant features. *Remote Sensing of Environment*, *26*, 1–16.

Schowengerdt, R. A. (1997). *Remote sensing models and methods for image processing*. 2nd edition. San Diego, CA: Academic Press Ltd.

Skole, D., & Tucker, C. (1993). Tropical deforestation and habitat fragmentation in the Amazon — Satellite data from 1978 to 1988. *Science*, *260*, 1905–1909.

Song, C., Woodcock, C. E., Seto, K. C., Lenney, M. P., & Macomber, S. A. (2001). Classification and change detection using Landsat TM data: When and how to correct atmospheric effects? *Remote Sensing of Environment*, *75*, 230–244.

Spanner, M., Johnson, L., Miller, J., McCreight, R., Freemantle, J., & Runyon, J., et al. (1994). Remote sensing of seasonal leaf area index across the Oregon transect. *Ecological Applications*, *4*, 258–271.

Spanner, M. A., Pierce, L. L., Peterson, D. L., & Running, S. W. (1990). Remote sensing of temperate coniferous forest leaf area index — The influence of canopy closure, understory vegetation and background reflectance. *International Journal of Remote Sensing*, *11*, 95–111.

Stow, D., Daeschner, S., Hope, A., Douglas, D., Myneni, R., & Tucker, C. (2001). Spatial–temporal trend of seasonally-integrated normalized difference vegetation index as an indicator of changes in arctic tundra vegetation in the early 1990s. *Proceedings of the international geoscience and remote sensing symposium, Sydney, Australia, July 2001*, *vol. 1* (pp. 181–183). Piscataway, new Jersey: IEEE.

Stow, D., Daeschner, S., Hope, A., Douglas, D., Petersen, A., & Myneni, R., et al. (2003). Variability of the seasonally integrated normalized difference vegetation index across the north slope of Alaska in the 1990s. *International Journal of Remote Sensing*, *24*(5), 1111–1117.

Xiao, X., Braswell, B., Zhang, Q., Boles, S., Frolking, S., & Moore III, B. (2003). Sensitivity of vegetation indices to atmospheric aerosols: Continental-scale observations in northern Asia. *Remote Sensing of Environment*, *84*, 385–392.